AMERICAN SOCIETY FOR MICROBIOLOGY | Journal of Virology®

VACCINES AND ANTIVIRAL AGENTS

Development of Reverse Genetics for the Prototype New World Mammarenavirus Tacaribe Virus

Chengjin Ye,[a] Juan Carlos de la Torre,[b] Luis Martínez-Sobrido[a]

[a]Texas Biomedical Research Institute, San Antonio, Texas, USA
[b]Department of Immunology and Microbiology, The Scripps Research Institute, La Jolla, California, USA

ABSTRACT The New World mammarenavirus Tacaribe virus (TCRV) has been isolated from fruit bats, mosquitoes, and ticks, whereas all other known New World mammarenaviruses are maintained in rodents. TCRV has not been linked to human disease, but it has been shown to protect against Argentine hemorrhagic fever-like disease in marmosets infected with the New World mammarenavirus Junín virus (JUNV), indicating the potential of TCRV as a live-attenuated vaccine for the treatment of Argentine hemorrhagic fever. Implementation of TCRV as a live-attenuated vaccine or a vaccine vector would be facilitated by the establishment of reverse genetics systems for the genetic manipulation of the TCRV genome. In this study, we developed, for the first time, reverse genetics approaches for the generation of recombinant TCRV (rTCRV). We successfully rescued a wild-type (WT) rTCRV (a trisegmented form of TCRV expressing two reporter genes [r3TCRV]) and a bisegmented TCRV expressing a single reporter gene from a bicistronic viral mRNA (rTCRV/GFP). These reverse genetics approaches represent an excellent tool to investigate the biology of TCRV and to explore its potential use as a live-attenuated vaccine or a vaccine vector for the treatment of other viral infections. Notably, we identified a 39-nucleotide (nt) deletion (Δ39) in the noncoding intergenic region (IGR) of the viral large (L) segment that is required for optimal virus multiplication. Accordingly, an rTCRV containing this 39-nt deletion in the L-IGR (rTCRV/Δ39) exhibited decreased viral fitness in cultured cells, suggesting the feasibility of using this deletion in the L-IGR as an approach to attenuate TCRV, and potentially other mammarenaviruses, for their implementation as live-attenuated vaccines or vaccine vectors.

IMPORTANCE To date, no Food and Drug Administration (FDA)-approved vaccines are available to combat hemorrhagic fever caused by mammarenavirus infections in humans. Treatment of mammarenavirus infections is limited to the off-label use of ribavirin, which is partially effective and associated with significant side effects. Tacaribe virus (TCRV), the prototype member of the New World mammarenaviruses, is nonpathogenic in humans but able to provide protection against Junín virus (JUNV), the causative agent of Argentine hemorrhagic fever, demonstrating the feasibility of using TCRV as a live-attenuated vaccine vector for the treatment of JUNV and potentially other viral infections. Here, we describe for the first time the feasibility of generating recombinant TCRV (rTCRV) using reverse genetics approaches, which paves the way to study the biology of TCRV and also its potential use as a live-attenuated vaccine or a vaccine vector for the treatment of mammarenavirus and/or other viral infections in humans.

KEYWORDS mammarenavirus, Tacaribe virus, reverse genetics, intergenic region, noncoding region, reporter virus, minigenome

Mammarenaviruses are enveloped RNA viruses with a bisegmented, negative-sense, single-stranded genome, which is composed of the small (S; ~3.5 kb) and the large (L; ~7.2 kb) segments (1). Each viral RNA (vRNA) segment encodes, using an

Citation Ye C, de la Torre JC, Martínez-Sobrido L. 2020. Development of reverse genetics for the prototype New World mammarenavirus Tacaribe virus. J Virol 94:e01014-20. https://doi.org/10.1128/JVI.01014-20.

Editor Rebecca Ellis Dutch, University of Kentucky College of Medicine

Address correspondence to Luis Martínez-Sobrido, lmartinez@txbiomed.org.

Received 22 May 2020
Accepted 2 July 2020
Accepted manuscript posted online 15 July 2020
Published 15 September 2020

ambisense coding strategy, two polypeptides in opposite orientations, separated by a noncoding intergenic region (IGR) (2, 3). Mammarenavirus IGR structures are predicted to form a stable stem-loop structure for transcription termination and have been described to be involved in enhancing viral gene expression (4). The viral nucleoprotein (NP) and the envelope glycoprotein precursor (GPC) are encoded by the S segment, whereas the L segment encodes the viral polymerase (L) protein and a small multifunctional matrix-like (Z) protein (5). GPC is cotranslationally cleaved by cellular signal peptidases to generate a 58-amino-acid-long stable signal peptide (SSP) and the immature GP1/2 precursor. The immature GP1/2 precursor is posttranslationally processed by the cellular protease subtilisin kexin isozyme-1 (SKI-1)/site 1 protease (S1P) to generate the mature virion surface glycoproteins GP1 and GP2 (6, 7). GP1, GP2, and SSP form a tripartite heterotrimeric GP complex that mediates virion receptor recognition and cell entry. GP1 is responsible for the binding of the virus to the host cell surface receptor, whereas GP2 directs a pH-dependent fusion event required to complete the virus entry process (8). NP and L are the minimum viral factors responsible for viral genome replication and transcription (9, 10). Mammarenavirus NPs have also been shown to be important virulence factors by inhibiting innate immune responses (11, 12). Z plays a critical role in virus budding from infected cells (13). It also negatively regulates the activity of the virus polymerase (13–15) and counteracts the host cell innate immune responses (16). Mammarenavirus L and S viral segments have highly conserved 3′ and 5′ terminal noncoding regions (NCR) that are predicted to form panhandle structures and serve as *cis*-acting elements or promoters required for viral transcription and replication (17).

Based on serologic and geographic distributions, mammarenaviruses are divided into two groups: New World, or Tacaribe virus (TCRV) complex, mammarenaviruses and Old World, or lymphocytic choriomeningitis virus (LCMV)/Lassa virus (LASV) complex, mammarenaviruses (18). Each mammarenavirus is associated with a particular rodent host species in which it is maintained (19). TCRV is an exception, since it was initially isolated from *Artibeus* bats and mosquitoes during a rabies surveillance survey conducted in Trinidad in 1956 (20). TCRV was also recently isolated from *Amblyomma americanum* ticks in Florida in 2013 (21). Six New World mammarenaviruses (Junin virus [JUNV], Machupo virus [MACV], Guanarito virus [GTOV], Sabia virus [SABV], Chapare virus [CHPV], and Ocozocoautla de Espinosa [OCEV]) and two Old World (LASV and Lujo virus [LUJV]) cause hemorrhagic fever disease in humans (22).

Live-attenuated vaccines, which often induce long-term protective immunity, have been successfully used to prevent viral infections. The live-attenuated Candid#1 strain, derived from the 44th mouse brain passage of the pathogenic XJ strain of JUNV, the causative agent of Argentine hemorrhagic fever (23), has been shown to be a safe and effective vaccine to reduce the number of Argentine hemorrhagic fever cases in areas where JUNV is endemic in the Argentine Pampas (24), and it is currently the only live-attenuated vaccine that has been used in humans to combat hemorrhagic fever-causing mammarenavirus infections. No other licensed mammarenavirus vaccines are available, and current antimammarenavirus therapy is limited to an off-label use of the broad-spectrum antiviral ribavirin, which has limited efficacy and is associated with adverse side effects (25, 26). Similar to Candid#1, TCRV protected guinea pigs and nonhuman primates against lethal challenge with JUNV (27), suggesting the feasibility of using TCRV, which is nonpathogenic to humans (28), as a natural live-attenuated vaccine to combat Argentine hemorrhagic fever.

Reverse genetics approaches facilitate the generation of attenuated forms of pathogenic viruses as live-attenuated vaccine candidates (29). Reverse genetics systems for the manipulation and generation of recombinant mammarenaviruses, including LCMV (30), LASV (31, 32), LUJV (33), JUNV (34), Pichinde virus (PICV) (35), and MACV (36), have been described. In this study, we describe for the first time the development of reverse genetics for the generation of recombinant TCRV (rTCRV). We rescued wild-type (WT) rTCRV, which is a trisegmented rTCRV expressing the green fluorescent protein (GFP) and *Gaussia* luciferase (Gluc) reporter genes (r3TCRV), and a bisegmented rTCRV

A)

S segment

Virus	Accession No.	5′ end	3′ end
LCMV	AY847350	CGCACCGGGGATCCTAGGCTTTT	GCCTAGGATCCACTGTGCG
Candid#1	LC066214	CGCACCGGGGATCCTAGGCGATT	GCCTAGGATCCACTGTGCG
TCRV Argentina	NC_004293	GGCATTT	GCCTAGGATCCACTGTGCG
TCRV Florida	KF923400	GGCATTT	GCCTAGGATCCACTGTGCG
TCRV BEI	M20304	GGCATTTCTTGTCCATATTT	GCCTAGGATCCACTGTGCG
TCRV BEI	TRVL-11573	CGCACCGGGGATCCTAGGCATTT	GCCTAGGATCCACTGTGCG

B)

L segment

Virus	Accession No.	5′ end	3′ end
LCMV	AY847351	CGCACCGGGGATCCTAGGCGT	GCCTAGGATCCTCGGTGCG
Candid#1	AY819707	CGCACCGGGGATCCTAGGCGT	GCCTAGGATCCTCGGTGCG
TCRV Argentina	NC_004292	CGCACCGGGGATCCTAGGCGT	GCCTAGGATCCACTGTGCG
TCRV Florida	KF923401	CGCACCGGGGATCCTAGGCGT	GCCTAGGATCCACTGTGCG
TCRV BEI	J04340	CGCACCGGGGATCCTAGGCGT	GCCTAGGATCCACTGTGCG
TCRV BEI	TRVL-11573	CGCACCGGGGATCCTAGGCGT	GCCTAGGATCCTCGGTGCG

FIG 1 Comparison of the 5′ and 3′ end NCR sequences of TCRV TRVL-11573 S (A) and L (B) with LCMV, Candid#1, and TCRV sequences deposited in PubMed. Differences between TCRV S (A) and L (B) segments from this study (TRVL-11573) and those deposited in the NCBI database are shown in red.

expressing GFP (rTCRV/GFP). We also identified a 39-nucleotide (nt) deletion in the TCRV L-IGR that resulted in reduced expression of reporter genes located in the Z locus yet did not affect their expression from the L locus. Moreover, we rescued an rTCRV containing this 39-nt deletion in the L-IGR (rTCRV/Δ39) and showed that rTCRV/Δ39 had reduced viral replication in cultured cells, suggesting the feasibility of using this approach for the generation of attenuated rTCRV as a live-attenuated vaccine or a vaccine vector. Also, a similar strategy could be implemented with other Old World and New World mammarenavirus to develop live-attenuated vaccines for their use in humans. This is the first description of a reverse genetics system for the rescue of viable rTCRV that can facilitate future investigations on viral tropism and transmission, as well as for the development of TCRV as a live-attenuated vaccine or a vaccine vector.

RESULTS

Verification of TCRV NCRs. Accurate viral genome sequence information, including that for noncoding regions (NCRs), is critical for the successful development of reverse genetics approaches. To confirm the complete S and L genome segment sequences of TCRV strain TRVL-11573 (NR-10175; Biodefense and Emerging Infections Research [BEI] Resources), we used next-generation sequencing (NGS) of vRNA isolated from purified TCRV virions. Our NGS results revealed significant differences with TCRV sequences deposited in the National Center for Biotechnology Information (NCBI) database (NC_004293, M20304, and KF923400 for S; NC_004292, J04340, and KF923401 for L), including 16 nt in the 5′ end of the S segment sequence that were missing or different in previously deposited TCRV sequences (Fig. 1A) and two nucleotide positions in the 3′ end NCR of the L segment (Fig. 1B).

Because of the critical role played by NCRs in viral genome replication and gene transcription of mammarenaviruses (9), we first examined whether the S and L NCRs obtained in our NGS analysis corresponded to functional sequences using a cell-based minigenome (MG) approach (9). In our MG assay, a virus-like RNA containing two reporter genes, GFP and Gluc, from either the S (Fig. 2A) or L (Fig. 2B) segment, is expressed under the control of a human polymerase (hPol-I) promoter. HEK293T cells were cotransfected with hPol-I-driven TCRV S or L antigenome MG1 (antiMG1) plasmids (Fig. 2A and B, respectively) and expression plasmids encoding hemagglutinin (HA)-tagged versions of TCRV L and NP to facilitate their detection (pCAGGS-HA-L and

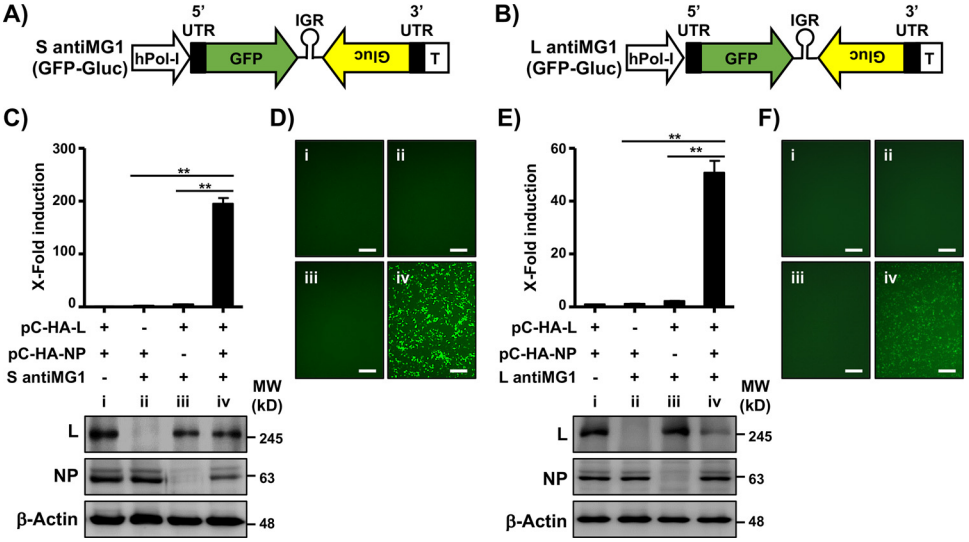

FIG 2 Verification of TCRV BEI TRVL-11573 S and L NCRs using an MG assay. (A and B) Schematic representation of TCRV S (A) and L (B) MG reporter-expressing plasmids. The backbone of the TCRV TRVL-11573 S and L, including 5′ and 3′ NCRs (black boxes) and IGRs (loops), was used to generate the MG reporter-expressing plasmids under the control of an hPol-I promoter and a mouse Pol-I (mPol-I) terminator I (T) sequence in antigenome (antiMG1) polarity. GFP was used to replace the viral NP (S segment) (A) and L (L segment) (B). Gluc was used instead of the GPC (S segment) (A) and Z (L segment) (B) viral genes. (C and D) TCRV S segment antiMG1 activity. HEK293T cells (6-well format, 10^6 cells/well, triplicates) were cotransfected with the indicated plasmids, together with pSV40-Cluc to normalize transfection efficiencies, and Gluc and Cluc activities in the tissue culture supernatants (C, top), and GFP expression (D) were determined at 48 h posttransfection. Lanes i to iv correspond to the plasmid combinations shown in panel C for HEK293T cell transfection. Bars, 100 μm. The changes in fold induction were calculated by normalizing the ratio of Gluc/Cluc in cells transfected in the absence of pCAGGS-HA-L to 1. Expression of TCRV L and NP from pCAGGS plasmids in transfected cells was analyzed by Western blotting using a monoclonal antibody against the HA epitope tag. A monoclonal antibody against β-actin was used as a loading control. Molecular weight (MW) markers in kilodaltons (kD) are indicated on the right (C, bottom). (E and F) TCRV L segment antiMG1 activity. HEK293T cells (6-well format, 10^6 cells/well, triplicates) were cotransfected with the indicated plasmids, together with pSV40 Cluc to normalize transfection efficiencies, and Gluc and Cluc in tissue culture supernatants (E, top) and GFP expression (F) were determined at 48 h posttransfection. Lanes i to iv correspond to the plasmid combinations shown in panel E for HEK293T cell transfection. Bars, 100 μm. The changes in fold induction were calculated by normalizing the ratio of Gluc/Cluc in cells transfected in the absence of pCAGGS-HA-L to 1. Expression levels of TCRV L and NP in transfected cells were analyzed by Western blotting using a monoclonal antibody against the HA epitope tag. β-Actin was used as a loading control. MW are indicated on the right (E, bottom). Data are means and SD. **, $P < 0.01$.

pCAGGS-HA-NP, respectively). At 48 h posttransfection, MG activities were evaluated by Gluc (Fig. 2C and E) and GFP (Fig. 2D and F) expression, and L and NP expression was confirmed by Western blotting using an antibody against the HA epitope tag (Fig. 2C and E, bottom). MGs containing the S and L segment NCRs of TCRV TRVL-11573 identified in our NGS efficiently directed both GFP and Gluc expression, with MG activity of the S antiMG1 (Fig. 2C and D) being higher than that of the L antiMG1 (Fig. 2E and F).

TCRV protein expression levels. We next evaluated MG-directed expression levels of reporter genes when they were expressed from the NP or GPC loci (S segment) as well as from the L or Z loci (L segment). To that end, we constructed S (Fig. 3A, bottom) and L (Fig. 4A, bottom) antiMG2, bearing the reporter genes in the loci opposite those in the S (Fig. 3A, top) and L (Fig. 4B, top) antiMG1. Relative expression levels of Gluc placed in the NP locus were higher than those obtained from the GPC locus in the S segment (Fig. 3B). Likewise, levels of Gluc expression from the Z locus were higher than those obtained from the L locus in the L segment (Fig. 4B). We obtained similar results when we evaluated GFP expression (Fig. 3C and 4C). These results suggested that expression levels of TCRV NP (S segment) and Z (L segment) proteins are greater than those of GPC and L, respectively (Table 1).

Rescue and characterization of rTCRV. Because the activity of the Pol-I promoter exhibits species specificity (37), we first evaluated the activity of the hPol-I promoter in

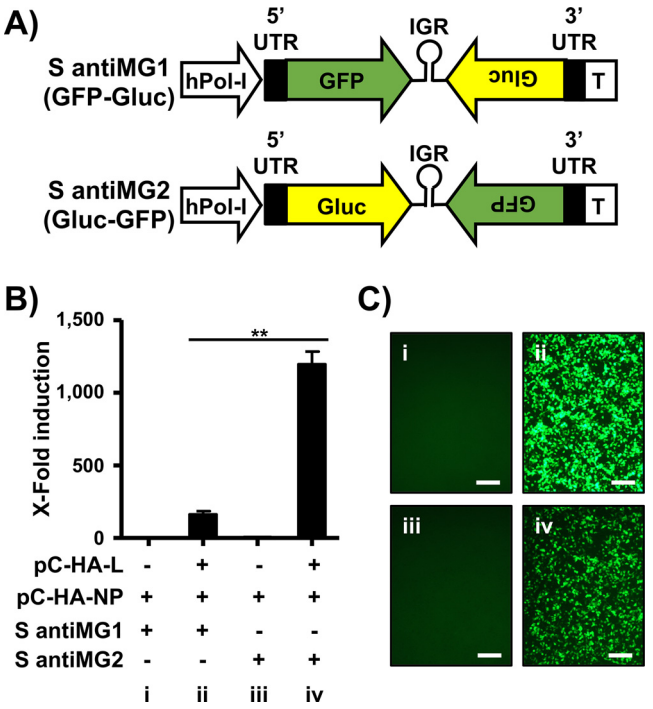

FIG 3 TCRV S segment protein expression levels. (A) Schematic representation of the TCRV S MG plasmids expressing GFP and Gluc reporter genes in different loci. The backbone of the TCRV S segment, including the 5′ and 3′ NCRs (black boxes) and IGR (loops), was used to generate the MG plasmids under the control of the hPol-I promoter and the mPol-I T in antigenome polarity. GFP and Gluc were used to replace TCRV NP and GPC (S antiMG1) or GPC and NP (S antiMG2). (B and C) Comparison of activity between S antiMG1 and S antiMG2. HEK293T cells (6-well format, 10^6 cells/well, triplicates) were cotransfected with the indicated plasmids, together with pSV40 Cluc to normalize transfection efficiencies. At 72 h posttransfection, Gluc and Cluc activities in the tissue culture supernatants from transfected cells (B) and GFP expression (C) were determined. Panels i to iv (C) correspond to the plasmid combinations shown in panel B for HEK293T cell transfection. Bars, 100 μm. Changes in fold induction were calculated by normalizing the ratio of Gluc/Cluc in the tissue culture supernatants of cells transfected with pCAGGS-HA-NP and S antiMG1 to 1 (no pCAGGS-HA-L). Data are means and SD. **, $P < 0.01$.

Vero cells. To that end, Vero cells were transfected with the hPol-I S antiMG1, together with pCAGGS-HA-L and pCAGGS-HA-NP. The TCRV S antiMG1 efficiently directed Gluc and GFP expression in Vero cells (Fig. 5A and B, respectively), although to a lesser extent than in HEK293T cells (Fig. 2 and 3), which likely reflected the lower transfection efficiency of Vero cells than HEK293T cells. Importantly, we confirmed the expression of TCRV L and NP by Western blotting (Fig. 5C).

To rescue rTCRV, we cloned the S and L TCRV segments in antigenome polarity downstream of the hPol-I promoter (Fig. 5D) and then cotransfected Vero cells with the TCRV S and L vRNA hPol-I-expressing plasmids, together with pCAGGS-HA-L and pCAGGS-HA-NP. At 72 h posttransfection, we passaged the cells and cultured them for 72 h prior to collecting tissue culture supernatants, which we used to infect fresh Vero cell monolayers. At 6 days postinfection, we collected tissue culture supernatants and determined production of infectious rTCRV progeny by immunofluorescence using a monoclonal antibody against JUNV NP (NR-2583; BEI Resources) that cross-reacts with TCRV NP. Mock-infected and TRVL-11573 (TCRV/WT)-infected Vero cells were used as negative and positive controls, respectively (Fig. 5E).

Next, we characterized rTCRV and compared it with its parental counterpart, TCRV/WT (Fig. 6). TCRV/WT and rTCRV formed plaques of similar sizes (2.6 $\pm$ 0.6 mm and 2.4 $\pm$ 0.5 mm, respectively) (Fig. 6A) and also exhibited comparable growth kinetics and viral peak titers (Fig. 6B). To confirm the genetic identity of both viruses, we amplified by reverse transcription-PCR (RT-PCR) an L region comprising nt 4,427 to 6,188 using RNA isolated from TCRV/WT- and rTCRV-infected Vero cells and digested

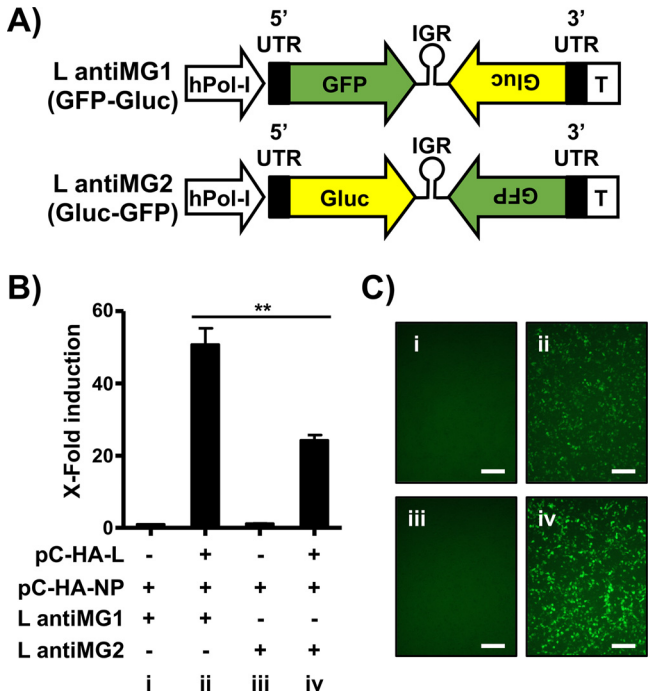

FIG 4 TCRV L segment protein expression levels. (A) Schematic representation of the TCRV L MG plasmids expressing GFP and Gluc reporter genes. The backbone of the TCRV L segment, including the 5′ and 3′ NCRs (black boxes) and IGR (loops), was used to generate the MG plasmids under the control of the hPol-I promoter and the mPol-I T in antigenome polarity. GFP and Gluc were used to replace TCRV L and Z (L antiMG1) or Z and L (L antiMG2). (B and C) Comparison of activity between L antiMG1 and L antiMG2. HEK293T cells (6-well format, 10^6 cells/well, triplicates) were cotransfected with the indicated plasmids, together with pSV40 Cluc to normalize transfection efficiencies. At 72 h posttransfection, Gluc and Cluc activities in the tissue culture supernatants from transfected cells (B) and GFP expression (C) were determined. Panels i to iv (C) correspond to the plasmid combinations shown in panel B for HEK293T cell transfection. Bars, 100 μm. Changes in fold induction were calculated by normalizing the ratio of Gluc/Cluc in the tissue culture supernatants of cells transfected in the absence of pCAGGS-HA-L to 1. Data are means and SD. **, $P < 0.01$.

the PCR products with BbsI. The BbsI restriction site present within this region in the L segment of TCRV/WT has been removed in rTCRV to serve as a genetic marker to distinguish TCRV/WT and rTCRV. Digestion of TCRV/WT, but not rTCRV, PCR product with BbsI resulted in the expected bands of 454 and 1,308 bp (Fig. 6C, bottom). We further confirmed the lack of the BbsI restriction site in the rTCRV PCR product by sequencing (Fig. 6D).

Generation and characterization of r3TCRV. Recombinant trisegmented (r3) mammarenaviruses expressing two foreign genes of interest (GOI) (e.g., Gluc and GFP genes) represent an excellent tool to study different aspects of the biology of these viruses (38). Several r3 mammarenaviruses have been described, including the prototype Old World mammarenavirus LCMV (39), and the New World mammarenavirus JUNV live-attenuated vaccine strain Candid#1 (34). To examine whether the use of this

TABLE 1 Relative expression level of TCRV proteins determined by MG[a]

Viral gene	Normalized expression level
NP	100
GPC	13.5 ± 1.1
L	2.0 ± 0.4
Z	4.3 ± 0.7

[a]The ratio of Gluc to Cluc was used to represent the relative expression level of viral genes located in different loci in the S (NP and GPC) and L (L and Z) viral segments. Levels of viral NP expression were given a relative value of 100. Expression of the other viral proteins was normalized to that of the NP. Values are means ± standard deviations.

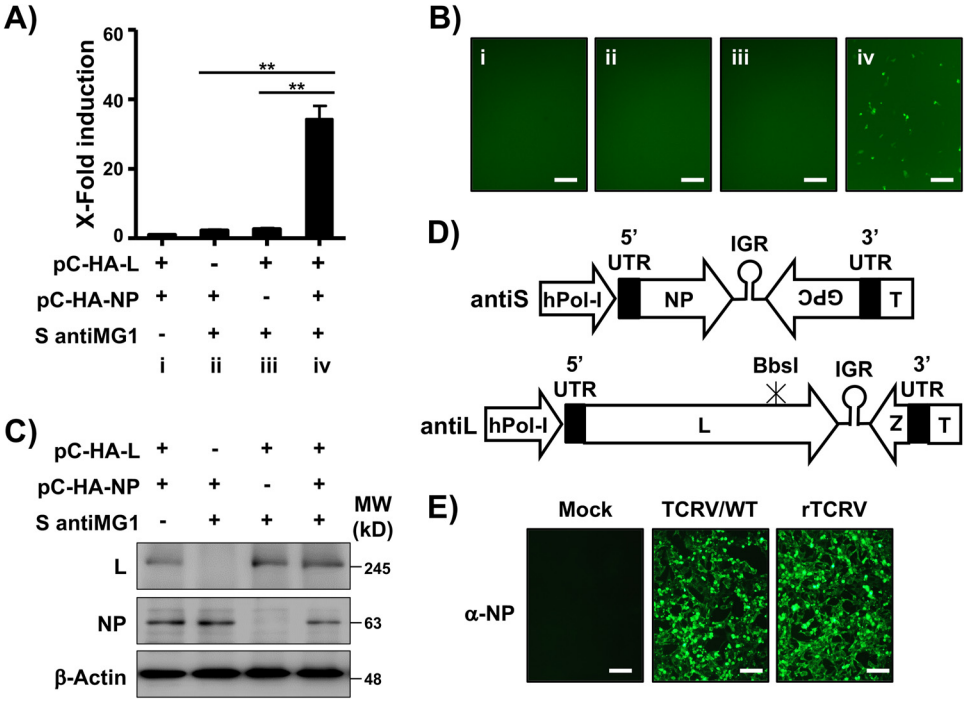

FIG 5 Rescue of rTCRV. (A to C) S antiMG1 activity in Vero cells. Vero cells (6-well format, 10^6 cells/well, triplicates) were cotransfected with the indicated plasmids and pSV40 Cluc to normalize transfection efficiencies, and Gluc and Cluc activities in the tissue culture supernatants (A) and GFP expression (B) were determined at 72 h posttransfection. Panels i to iv (B) correspond to the plasmid combinations shown in panel A for HEK293T cell transfection. Bars, 100 μm. Whole-cell lysates were subjected to Western blotting to evaluate TCRV HA-tagged L and NP expression levels using a monoclonal antibody against the HA epitope tag. β-Actin was probed as a loading control. MW are indicated on the right (C). Data are means and SD. **, $P < 0.01$. (D) Schematic representation of the hPol-I plasmids for rescue of rTCRV. The viral coding sequences of TCRV NP and GPC (S segment; top) or L and Z (L segment; bottom) were inserted into the backbone of the S and L segments, respectively, in antigenome polarity to generate the antiS and antiL plasmids for the expression of the antigenome S and L vRNA. A BbsI restriction site (nt 4878) was removed by silent mutation as a genetic tag. Black boxes indicate the 5′ and 3′ NCRs. IGRs are indicated as loops. The positions of the hPol-I promoter and the mPol-I T are also indicated. (E) Rescue of rTCRV. Vero cells (6-well format, 10^6 cells/well, triplicates) were cotransfected with the antiS and antiL plasmids (D), together with the pCAGGS plasmids expressing TCRV HA-L and HA-NP. At 72 h posttransfection, cells were split into 100-mm dishes and incubated for an additional 72 h. Tissue culture supernatants were collected and used to infect fresh Vero cells for 96 h. Infected cells were identified by immunostaining using a JUNV NP cross-reactive monoclonal antibody. Mock-infected and TCRV/WT-infected cells were included as negative and positive controls, respectively. Bars, 100 μm.

approach could be extended to TCRV, we used the strategy described for LCMV (39) and Candid#1 (34) to generate r3TCRV. In this r3 approach, the viral NP and GPC in the S segment are split into two S segments (S1 and S2), each of them encoding a viral protein and containing a reporter gene. We generated two hPol-I plasmids expressing an S1 segment encoding GFP instead of NP (antiS1) and an S2 segment encoding Gluc instead of GPC (antiS2) (Fig. 7A). To generate the r3TCRV, we cotransfected Vero cells with the antiS1, antiS2, and antiL plasmids, together with the pCAGGS-HA-L and pCAGGS-HA-NP. At 72 h posttransfection, we passaged the cells and cultured them for 72 h prior to collecting tissue culture supernatants, which were used to infect fresh Vero cells for 6 days. We next performed plaque assays to visualize the plaques of r3TCRV and compare them to those of rTCRV using fluorescence microscopy and immunostaining with the JUNV NP cross-reactive monoclonal antibody. As expected, we observed GFP-expressing plaques in cells infected with r3TCRV but not in those infected with rTCRV (Fig. 7B, left). We detected viral plaques in both r3TCRV- and rTCRV-infected cells immunostained with the NP monoclonal antibody (Fig. 7B, right). Plaques formed by r3TCRV (1.1 ± 0.3 mm) were smaller than those of rTCRV (2.4 ± 0.5 mm). Consistent with a reduced plaque size, r3TCRV exhibited, compared to

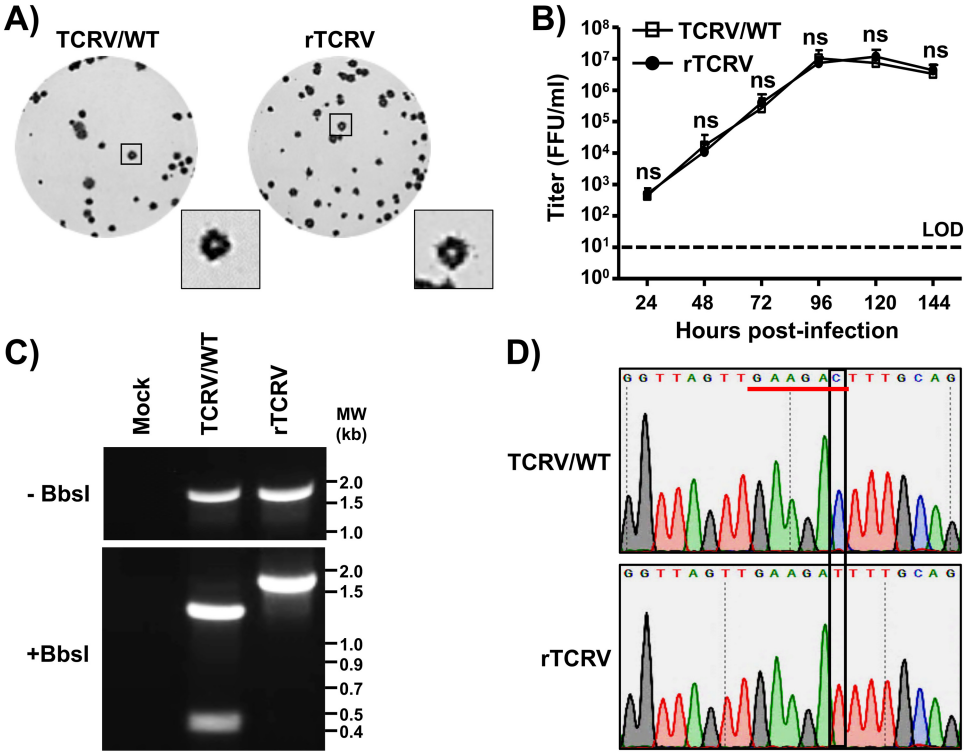

FIG 6 Characterization of the rTCRV. (A) Plaque phenotype: Vero cells (6-well format, 10^6 cells/well) were infected with ~25 to 50 PFU of TCRV/WT (left) or rTCRV (right) for 1 h at 37°C. After viral absorption, cells were washed 3 times with PBS and overlaid with 3 ml of DMEM–2.5% FBS containing 0.1% agarose and cultured at 37°C. After 6 days, cells were fixed and immunostained with a JUNV NP cross-reactive monoclonal antibody. (B) Growth kinetics. Vero cells (6-well format, 10^6 cells/well, triplicate) were infected (MOI = 0.01) with TCRV/WT or rTCRV for 1 h at 37°C. After viral absorption, cells were washed 3 times with PBS and incubated in DMEM–2.5% FBS. At the indicated times p.i., tissue culture supernatants were collected and viral titers were assessed by immunofocus assay. Data are means ± SD. ns, not significant; LOD, limit of detection. (C and D) Genotypic characterization of rTCRV. Vero cells (6-well format, 10^6 cells/well) were mock infected or infected (MOI = 0.01) with TCRV/WT or rTCRV for 1 h. After viral absorption at 37°C, cells were washed 3 times with PBS and incubated in DMEM–2.5% FBS at 37°C. At 72 h postinfection, total RNA was extracted and RT-PCR was used to amplify a 1,762-nt region from nt 4427 to 6188 in the L segment. Amplified cDNA was subjected to BbsI digestion. Undigested and BbsI-digested samples were separated in a 0.7% agarose gel (C). Amplified cDNA was sequenced to verify the presence of the silent mutation in the BbsI restriction site in the genome of rTCRV. The BbsI restriction site is underlined in red, and the mutation introduced to remove the BbsI restriction site (C to T) is shown in the black box (D).

TCRV/WT, decreased growth fitness in cultured cells (Fig. 7C). As expected, Gluc was detected only in the tissue culture supernatants of cells infected with r3TCRV (Fig. 7D).

Rescue and characterization of a bisegmented reporter rTCRV/GFP. Porcine teschovirus-1 2A (P2A) is a 19-amino-acid long peptide that can induce high-efficiency self-cleavage of recombinant proteins in mammalian cells (40, 41). Recently, the P2A proteolytic cleavage site was used to generate recombinant LCMV (42) and LASV (43) Old World mammarenaviruses that express a single reporter gene from a bisegmented genome. We tested the feasibility of using the P2A strategy to generate a bicistronic rTCRV/GFP. To that end, we generated an antiS′ plasmid in which GFP was fused to the N terminus of TCRV NP and separated by a P2A cleavage site (Fig. 8A). We then cotransfected Vero cells with the hPol-I vRNA expressing antiS′ and antiL plasmids, together with pCAGGS-HA-L and pCAGGS-HA-NP. At 72 h posttransfection, we passaged the cells and cultured them for 72 h prior to collecting tissue culture supernatants and using them to infect fresh Vero cells for 6 days. In plaque assays, cells infected with rTCRV/GFP, but not with rTCRV, expressed GFP (Fig. 8B, left), while both rTCRV/GFP and rTCRV plaques were immunostained with the JUNV NP monoclonal antibody (Fig. 8B, right). Plaque sizes formed by rTCRV/GFP (1.2 ± 0.2 mm) were smaller than those of rTCRV (2.6 ± 0.4 mm). Importantly, rTCRV/GFP replicated only slightly less efficiently

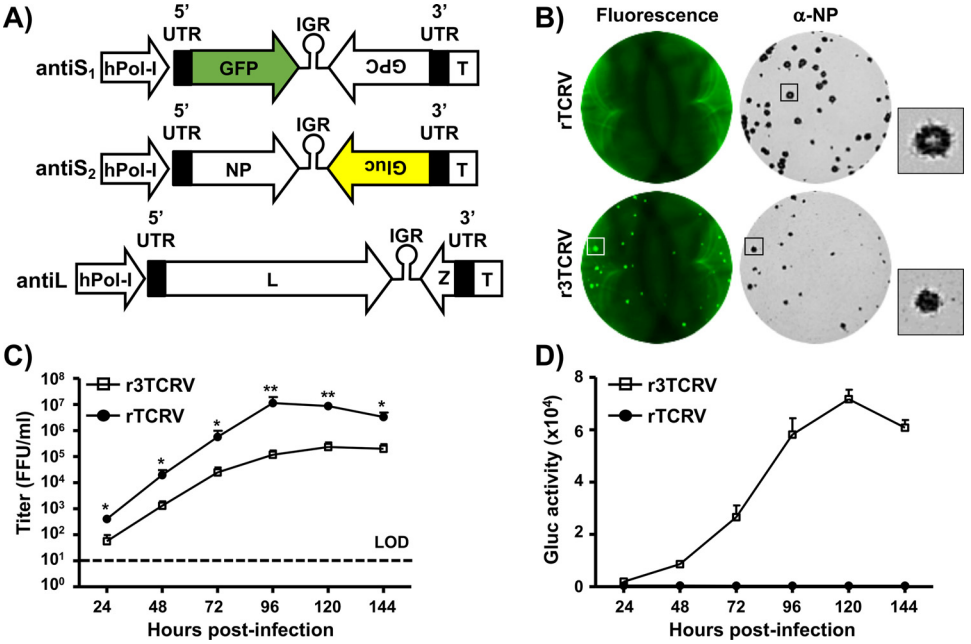

FIG 7 Generation and characterization of r3TCRV. (A) Schematic representation of the plasmids used for the generation of r3TCRV. The antiS1 and antiS2 plasmids for the expression of S1 and S2 TCRV viral segments in antigenome polarity were generated from the antiS plasmid (Fig. 5D) by replacing NP with GFP and GPC with Gluc. Black boxes indicate the 5′ and 3′ NCRs. IGRs are indicated as loops. The positions of the hPol-I promoter and the mPol-I T are also indicated. (B) Plaque phenotype. Vero cells (6-well format, 10^6 cells/well) were infected with ~25 to 50 FFU of rTCRV (top) or r3TCRV (bottom) for 1 h at 37°C. After viral absorption, cells were washed 3 times with PBS and cultured with DMEM–2.5% FBS and 0.1% agarose at 37°C. Six days after infection, plaques were visualized using a ChemiDoc MP imaging system, and images were taken using light with 488-nm excitation. After fluorescence visualization, cells were fixed, permeabilized, and immunostained with the anti-JUNV NP cross-reactive monoclonal antibody. (C) Growth kinetics. Vero cells (6-well format, 10^6 cells/well, triplicates) were infected (MOI = 0.01) with r3TCRV or rTCRV. After viral absorption at 37°C, cell monolayers were washed 3 times with PBS and overlaid with DMEM–2.5% FBS. At the indicated time postinfection, tissue culture supernatants were collected and presence of the virus was determined by immunofocus assay. (D) Gluc expression. Vero cells (6-well format, 10^6 cells/well, triplicates) were infected (MOI = 0.01) with r3TCRV or rTCRV for 1 h. After viral infection at 37°C, cells were washed 3 times with PBS and incubated in DMEM–2.5% FBS. At the indicated times postinfection, tissue culture supernatants were collected, and the presence of Gluc was evaluated using a Gluc assay. Data are means ± SD. *, $P < 0.05$; **, $P < 0.01$.

(~0.5 log) than rTCRV in Vero cells (Fig. 8C). In addition, rTCRV/GFP exhibited, compared to r3TCRV, faster growth kinetics and higher peak viral titers in Vero cells (Fig. 8D).

Effect of a 39-nt deletion in the L-IGR on TCRV MG activity. Mammarenavirus IGRs have been shown to mediate transcription termination of viral mRNAs (3, 4, 44). We used an online program (RNAstructure) to predict the secondary structure of TCRV L-IGR based on a model of minimum free energy. The WT L-IGR in antigenome polarity (Fig. 9A, top) was predicted to form a three-stem-loop structure (Fig. 9B, top). Based on the predicted secondary structure of the TCRV L-IGR, we generated an L-IGR with 39 nt deleted (IGR/Δ39) that was G/C rich (Fig. 9A, bottom) and predicted to form a two stem-loop structure (Fig. 9B, bottom). To assess how the deletion of these 39 internal nucleotides in L-IGR affected TCRV genome replication and gene transcription, we first tested the activity of the corresponding MGs (antiMG1/Δ39 and antiMG2/Δ39). Gluc activity from the Z locus directed by L antiMG1/Δ39 was decreased ~60% compared to that of the WT L antiMG1 (Fig. 9C). In contrast, both antiMG2/Δ39 and antiMG2 directed similar levels of Gluc activity from the L locus (Fig. 9C). Gluc results were consistent with those obtained using GFP expression as the readout (Fig. 9D).

Rescue and characterization of rTCRV/Δ39. Given that expression of reporter genes from the Z locus, but not from the L locus, was significantly decreased in MGs containing an internal 39-nt deletion within the L-IGR, we next attempted to rescue an

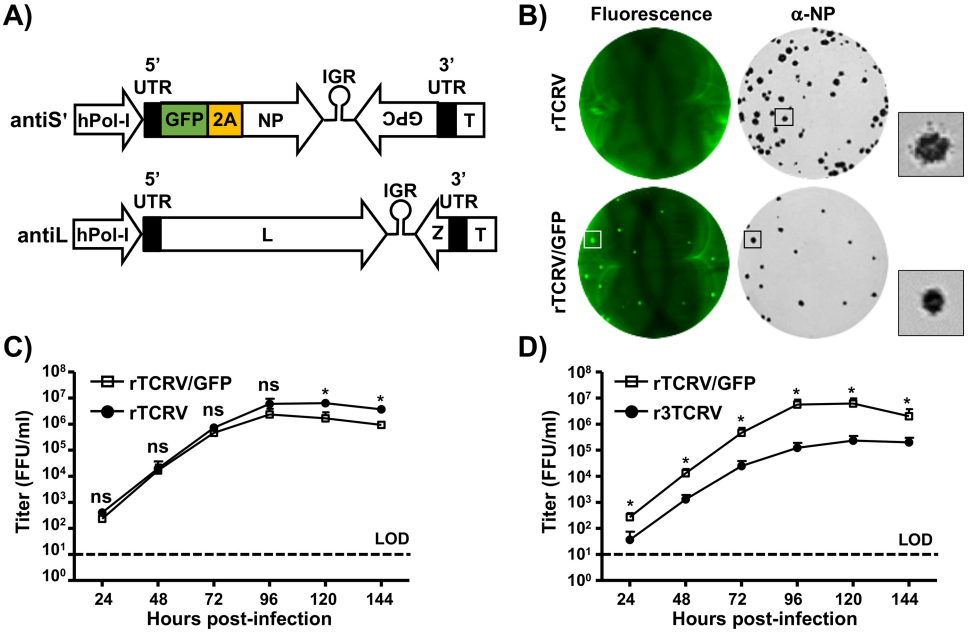

FIG 8 Rescue and characterization of rTCRV/GFP. (A) Schematic representation of the plasmids used for generation of rTCRV/GFP. The antiS′ plasmid was generated by genetically cloning the open reading frame of GFP and the P2A proteolytic cleavage site in front of TCRV NP. Black boxes indicate the 5′ and 3′ NCRs. IGRs are indicated as loops. The position of the hPol-I promoter and the mPol-I T are also indicated. (B) Plaque phenotype. Vero cells (6-well format, 10^6 cells/well) were infected with ~25 to 50 FFU of rTCRV (top) or rTCRV/GFP (bottom) for 1 h at 37°C. After viral absorption, cell monolayers were washed 3 times with PBS and overlaid with DMEM–2.5% FBS containing 0.1% agarose for 6 days at 37°C. Plaques were visualized with a ChemiDoc MP imaging system, and images were taken using light with 488-nm excitation. After fluorescence visualization, cells were fixed, permeabilized, and immunostained with the anti-JUNV NP cross-reactive monoclonal antibody. (C) Growth kinetics. Vero cells (6-well format, 10^6 cells/well, triplicates) were infected (MOI = 0.01) with rTCRV/GFP or rTCRV for 1 h. After viral infection at 37°C, cells were washed 3 times with PBS and incubated with DMEM 2.5%–FBS. At the indicated times postinfection, tissue culture supernatants were collected, and the presence of the virus was assessed by immunofocus assay. (D) Comparison of rTCRV/GFP and r3TCRV growth kinetics. Vero cells (6-well format, 10^6 cells/well, triplicates) were infected (MOI = 0.01) with rTCRV/GFP or r3TCRV for 1 h at 37°C. After viral absorption, cell monolayers were washed 3 times with PBS and incubated in DMEM–2.5% FBS. At the indicated times postinfection, tissue culture supernatants were collected, and the presence of the virus was assessed by immunofocus assay. Data are means ± SD. *, $P < 0.05$; ns, not significant.

rTCRV containing this 39-nt deletion (rTCRV/Δ39). We rescued rTCRV/Δ39, which exhibited a significant decrease in viral fitness, reflected by its reduced plaque size (0.3 ± 0.1 mm) compared to that of rTCRV (2.6 ± 0.6 mm) (Fig. 10A) and its slower growth kinetics and reduced (~3 logs) peak titers (Fig. 10B). Importantly, we confirmed the 39-nt deletion in the L-IGR of rTCRV/Δ39 by gel electrophoresis (Fig. 10C) and sequencing (Fig. 10D).

DISCUSSION

Reverse genetics systems have already been developed for several Old World and New World mammarenavirus, including LCMV (30), LASV (31, 32), LUJV (33), JUNV (34), PICV (35), and MACV (36). However, to date, reverse genetics approaches to generate rTCRV, the prototype member of the New World mammarenavirus, or TCRV, complex have not been described. To develop a reverse genetics system for TCRV, we first confirmed the identity of the viral 5′ and 3′ NCRs and IGR sequences in the S and L viral segments by using vRNA isolated from purified TCRV virions produced in Vero cells for NGS. Unexpectedly, our newly determined TCRV sequence revealed differences, compared to previously reported TCRV sequences, within the 5′- and 3′-end NCRs of the S and L segments, respectively (Fig. 1). We next verified the functionality of the newly determined sequences using our cell-based MG system (Fig. 2). Consistent with findings with other mammarenaviruses, reporter gene expression levels were higher from the NP than the GPC locus in the S segment S (Fig. 3) and higher from the Z than L locus

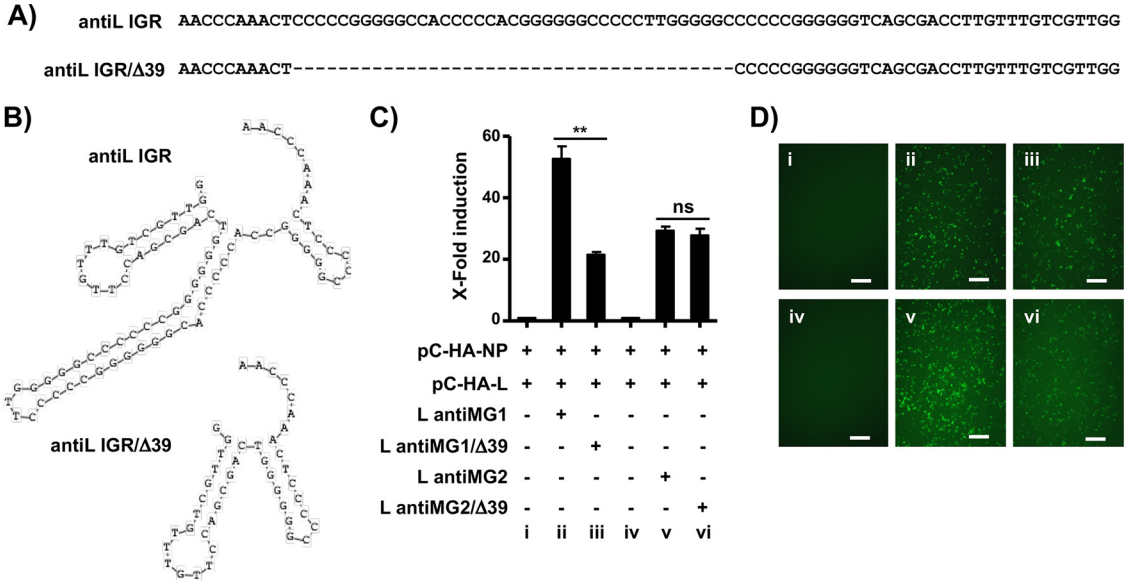

FIG 9 Effect of a 39-nt deletion in the TCRV L-IGR in viral replication and transcription. (A) WT (top) and 39-nt deletion (bottom) TCRV L segment IGR sequences. The dashed line indicates the 39-nt deletion in the IGR/Δ39 TCRV L-IGR. (B) Predicted secondary structures of WT (top) and Δ39 (bottom) TCRV L-IGR. (C and D) Effect of Δ39 on MG activity. HEK293T cells (6-well format, 10^6 cells/well, triplicates) were cotransfected with the indicated plasmids, together with pSV40-Cluc to normalize transfection efficiencies. At 72 h posttransfection, Gluc and Cluc activities in the tissue culture supernatants (C) and GFP expression (D) were measured. Panels i to vi (D) correspond to the plasmid combinations shown in panel C for HEK293T cell transfection. Bars, 100 μm. Fold induction of Gluc was calculated by normalizing the ratio of Gluc/Cluc in the tissue culture supernatants of cell transfected with in the absence of pCAGGS-HA-L. Data are means and SD. **, $P < 0.01$; ns, not significant.

in the L segment (Fig. 4). We then used our hPol-I reverse genetics system to generate rTCRV (Fig. 5 and 6), r3TCRV (Fig. 7), rTCRV/GFP (Fig. 8), and a mutant rTCRV containing a 39-nt deletion in the L-IGR (rTCRV/Δ39) (Fig. 9), which exhibited, compared to rTCRV, an attenuated growth kinetic phenotype in Vero cells (Fig. 10). We did not determine the complete genome sequence of rTCRV/Δ39, and therefore we cannot formally rule out the possibility that during the rescue and amplification of rTCRV/Δ39, additional mutations were incorporated into the viral genome and contributed to the attenuated phenotype of rTCRVΔ39. However, there is evidence that altered expression from the Z locus due to changes in the L-IGR is associated with viral attenuation (45), and the IGR has been shown to play a critical role in the production of infectious particles (4). These findings support the idea that the 39-nt deletion within the L-IGR is mainly, or solely, responsible for the attenuated phenotype of rTCRV/Δ39.

Since TCRV was first identified in 1956 (20), novel New World mammarenaviruses have been discovered every 1 to 3 years, including several causative agents of hemorrhagic fever (HF) disease in humans, such as JUNV, isolated in 1958, the causative agent of Argentine HF (46), and MACV, isolated in 1959, the causative agent of Bolivian HF (47). More recently identified HF-causing New World mammarenavirus are GTOV, isolated in Venezuela in 1989 (48), SABV, isolated in Brazil in 1993 (49), CHPV, isolated in Bolivia in 2004 (50), and OCEV, isolated in Mexico in 2010 (51). The geographic distribution of mammarenaviruses is determined by that of the rodent species serving as natural reservoirs. A unique exception is TCRV, which was not isolated from rodents but rather from fruit bats (20), mosquitoes (20), and ticks (21). The TCRV genomic sequences of a tick-isolated Florida strain and the bat-isolated BEI TRVL-11573 strain used in this study share more than 99% identity in the S segment coding sequences (Table 2) and 100% identity in the L coding sequences (Table 3), at both the nucleotide and amino acid levels, indicating that they represent isolates of the same strain. Viral zoonosis can be greatly facilitated by the contribution of arthropod vectors in the natural history of the virus, which could contribute to human infections by TCRV or TCRV-like viruses. Human-pathogenic New World mammarenaviruses enter cells using

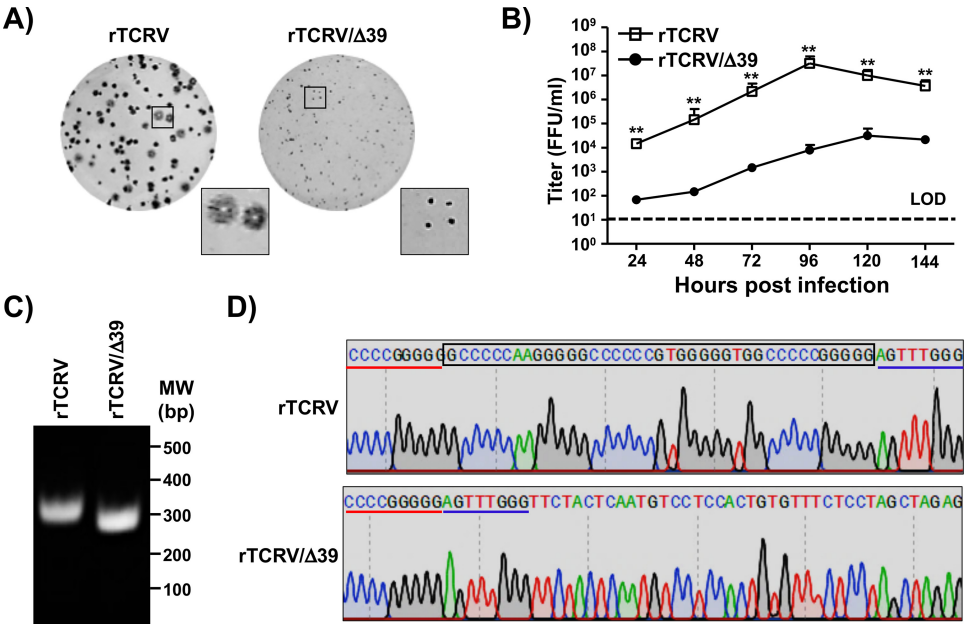

FIG 10 Rescue and characterization of rTCRV/Δ39. (A) Plaque phenotype. Vero cells (6-well format, 10^6 cells/well) were infected with ~25 to 50 FFU of rTCRV (left) or rTCRV/Δ39 (right) for 1 h at 37°C. After viral infection, cells were washed 3 times with PBS and overlaid with DMEM–2.5% FBS containing 0.1% agarose for 6 days at 37°C. (B) Growth kinetics. Vero cells (6-well format, 10^6 cells/well, triplicates) were infected (MOI = 0.01) with rTCRV or rTCRV/Δ39 for 1 h. After viral absorption at 37°C, cell monolayers were washed 3 times with PBS and incubated with DMEM–2.5% FBS. At the indicated times postinfection, tissue culture supernatants were collected, and the presence of the virus was determined by immunofocus assay. Data are means ± SD. **, $P < 0.01$. (C and D) Genotypic characterization of rTCRV/Δ39: Vero cells (6-well format, 10^6 cells/well) were infected (MOI 0.01) with rTCRV or rTCRV/Δ39 for 1 h at 37°C, and after viral absorption, cell monolayers were washed 3 times with PBS and incubated with DMEM–2.5% FBS at 37°C. At 72 h postinfection, total RNA was extracted, and RT-PCR was used to amplify a 344-nt region (nt 7896 to 8239) that includes the TCRV L-IGR. Amplified cDNAs were separated in a 0.7% agarose gel (C). Amplified cDNA was sequenced to verify the presence of the 39-nt deletion in the TCRV L segment IGR in rTCRV/Δ39 (D). The 39-nt deleted L-IGR region is shown in the black box. The surrounding 5′ and 3′ regions are underlined in red and blue, respectively (D).

human transferrin receptor 1 (hTfR1) (28). TCRV does not use hTfR1 as a main cell entry receptor, and evidence suggests that TCRV is nonpathogenic for humans. However, a single amino acid substitution in hTfR1 allowed its use as a cell entry receptor by TCRV (28), suggesting that few changes in the virus receptor binding protein, upon extended use in humans, might render TCRV as virulent as other highly pathogenic clade B New World mammarenaviruses. The ability to rescue rTCRV with predetermined mutations in its viral genome would facilitate a comprehensive assessment of the zoonotic potential of TCRV, as well as a detailed understanding of viral genetic determinants of attenuation and potential pathogenicity in humans.

To date, vaccination is still one of the most effective ways to prevent viral diseases, with live-attenuated vaccines having several advantages over inactivated vaccines to confer better protection against subsequent natural viral infections. The live-attenuated

TABLE 2 Identity of TCRV TRVL-11573 S segment with those deposited in the NCBI database[a]

	% Identity with TCRV TRVL-11573 S					
	TCRV Argentina (NC_004293)		TCRV Florida (KF923400)		TCRV BEI (M20304)	
Protein or region	Nucleotide	Amino acid	Nucleotide	Amino acid	Nucleotide	Amino acid
5′ NCR	75.00	NA	76.47	NA	74.63	NA
GPC	99.31	96.77	99.72	99.59	99.31	96.77
IGR	84.96	NA	100.00	NA	84.96	NA
NP	98.54	97.54	99.53	99.12	98.54	97.54
3′ NCR	100.00	NA	100.00	NA	100.00	NA

[a]NA, not applicable.

TABLE 3 Identity of TCRV TRVL-11573 L segment with those deposited in the NCBI database[a]

	% Identity with TCRV TRVL-11573 L					
	TCRV Argentina (NC_004292)		TCRV Florida (KF923401)		TCRV BEI (J04340)	
Protein or region	Nucleotide	Amino acid	Nucleotide	Amino acid	Nucleotide	Amino acid
5′ NCR	100.00	NA	100.00	NA	100.00	NA
Z	100.00	100.00	100.00	100.00	100.00	100.00
IGR	100.00	NA	100.00	NA	100.00	NA
L	99.79	99.55	100.00	100.00	99.79	99.55
3′ NCR	93.33	NA	93.33	NA	93.33	NA

[a]NA, not applicable.

vaccine strain Candid#1 has been shown to be a safe and effective vaccine to prevent cases of Argentine hemorrhagic fever among the population at risk in the region of the Argentine Pampas where JUNV is endemic (52). However, the mechanisms of Candid#1 attenuation are not fully understood, and the potential for additional mutations that might be incorporated into the Candid#1 genome and could result in virulence is supported by the observed variability in virulence among different clonal Candid#1 populations (53). Hence, development of live-attenuated mammarenavirus vaccines needs to be based on well-defined molecular mechanisms of attenuation. Recently, different strategies have been developed to generate attenuated forms of mammarenavirus for their implementation as live-attenuated vaccines. These include, among others, the use of codon-deoptimized NP (54) or GPC (55), the replacement of the L-IGR with the S-IGR (45), and the genome rearrangement of NP and GPC in the viral S segment (56). The concept that deletions within the intergenic region (IGR) of the L genome segment can result in attenuation of the mammarenaviruses MACV (57) and LUJV (33) has been documented. Here, we document that attenuation of TCRV via deletions in the L-IGR is associated with reduced levels of Z, but not L, protein expression, providing for the first time a molecular mechanism of attenuation caused by deletions in the L-IGR. Our results from cell-based MG assays suggest that a shorter L-IGR likely results in decreased expression levels of the viral Z protein without affecting L protein expression levels. TCRV has not been linked to human disease, and therefore, r3TCRV-expressing antigens from HF-causing New World mammarenavirus represent an attractive platform for a live-attenuated vaccine vector. Moreover, TCRV is not present in West Africa and it does not infect livestock, suggesting that r3TCRV-expressing antigens from HF-causing Old World mammarenavirus should be explored as potential live-attenuated vaccine candidates to combat LASV and other potential emerging HF-causing Old World mammarenaviruses.

MATERIALS AND METHODS

Cells and virus. Human embryonic kidney 293T (HEK293T, ATCC CRL-11268) and African green monkey kidney epithelial Vero (ATCC CCL-81) cells were maintained in Dulbecco's modified Eagle medium (DMEM) supplemented with 5% (vol/vol) fetal bovine serum (FBS; VWR) and 100 U/ml penicillin-streptomycin (Corning). All cells were cultured at 37°C in a humidified 5% CO_2 atmosphere incubator. TCRV (TRVL-11573; BEI Resources) was grown in Vero cells at 37°C.

RNA extraction and NGS. TCRV was expanded by infecting (multiplicity of infection [MOI] = 0.01) Vero cells (10^7 cells, 100-mm-dish format) for 120 h. Tissue culture supernatants was collected and clarified by centrifuging for 30 min at 3,000 × *g* at 4°C. The TCRV was crudely purified by ultracentrifugation at 30,000 × *g* for 3 h; the pellet was resuspended with TRIzol reagent (Thermo Fisher), and the viral RNA was extracted according to the manufacturer's instructions. NGS of the viral RNA was carried out at the Genomic Research Center of University of Rochester, and the sequence data were assembled and aligned by Integrative Genomic Viewer (IGV 2.4.18) (58). The entire TCRV genome sequences were synthesized *de novo* by Bio Basic (Ontario, Canada), based on the assembly of the NGS results.

Plasmids. The coding sequences of TCRV L and NP were subcloned into the pCAGGS-HA-NH2 plasmid (59), using conventional restriction sites. The viral genomic fragments were cloned into the hPol-I plasmid (37). MG plasmids based on the backbone of the TCRV S and L segments were constructed by cloning GFP and Gluc in lieu of the viral NP and GP (S segment) or the L and Z (L segment), as previously described (56). Deletion of the 39 nt in the segment L-IGR to generate the antiMG1/Δ39 and antiMG2/Δ39 plasmids was accomplished using inverse PCR (60). All plasmids were sequenced (ACGT) to ensure no unwanted mutations.

Antibodies. The mouse anti-JUNV NP monoclonal antibody PC01-AD12, which cross-reacts with TCRV NP, was obtained from BEI Resources (NR-2583). The mouse anti-actin monoclonal antibody was purchased from Abcam. The mouse anti-HA monoclonal antibody was purchased from Sigma-Aldrich. Fluorescein isothiocyanate (FITC)-labeled rabbit anti-mouse IgG and horseradish peroxidase (HRP)-labeled sheep anti-mouse IgG secondary antibodies were purchased from Agilent and GE Healthcare Life Sciences, respectively.

Western blots. Whole-cell lysates were prepared in passive lysis buffer (Promega) at 4°C for 30 min, followed by centrifugation (12,000 × *g*) at 4°C for another 30 min. Equivalent amounts of cell lysates were subjected to 12% SDS-PAGE and transferred to nitrocellulose membranes. After blocking with 5% (vol/vol) bovine serum albumin (BSA) in PBS containing 0.1% (vol/vol) Tween 20 (PBST) for 1 h, membranes were incubated at 4°C with primary antibodies overnight, followed by 3 washes with PBST and incubation at 37°C with an HRP-conjugated secondary antibody for 1 h. β-Actin was probed as a loading control. Blots were developed, after 3 washes with PBST, with enhanced chemiluminescence (ECL) detection reagent (Thermo Fisher) and analyzed using a ChemiDoc MP imaging system (Bio-Rad).

Immunofluorescence. Vero cells (10^6 cells/well, 6-well plate format, triplicates) were infected (MOI = 1) with TCRV/WT or rTCRV. At 96 h postinfection, cells were fixed with 4% (vol/vol) paraformaldehyde (PFA) in PBS at 4°C overnight and permeabilized using 0.5% (vol/vol) Triton X-100 in PBS for 15 min at room temperature. Cells were incubated with the JUNV NP monoclonal antibody (1 μg/ml) at 4°C overnight, washed with PBS, and stained with a FITC-labeled goat anti-mouse IgG (1:200). After washing with PBS, cells were visualized and imaged under a fluorescence microscope (Olympus).

Minigenome assays. MG assays were performed as previously described (61). Briefly, monolayers of HEK293T or Vero cells (10^6 cells/well, 6-well plate format, triplicates) were cotransfected, using Lipofectamine 2000 (LPF2000), with 2 μg of the S or L antiMG1 or antiMG2 expressing GFP and Gluc, 1 μg of pCAGGS-HA-L, 1 μg of pCAGGS-HA-NP, and 10 ng of a plasmid expressing *Cypridina* luciferase (Cluc) under the control of a polymerase II-dependent SV40 promoter (pSV40-Cluc). At 48 h posttransfection, luciferases activities in tissue culture supernatants of transfected cells were assessed using Gluc and Cluc detection kits (NEB) with a luciferase multiplate reader (Beckman) and normalized as previously described (37). GFP expression was visualized and imaged under a fluorescence microscope (Olympus).

Rescue of rTCRVs. Virus rescue experiments were performed as previously described (62). Briefly, confluent monolayers of Vero cells (10^6 cells/well, 6-well plate format, triplicates) were cotransfected, using LPF2000, with the pCAGGS-HA-L (1.0 μg/well) and pCAGGS-HA-NP (0.8 μg/well) expression plasmids and the TCRV S (or S′) and L hPol-I vRNA expression plasmids (0.8 μg/well and 1.4 μg/well, respectively) or TCRV S1, S2, and L hPol-I vRNA expression plasmids (0.8 μg/well, 0.8 μg/well, and 1.4 μg/well, respectively). At 72 h posttransfection, cells were split and seeded into 100-mm petri dishes. After incubation for another 72 h, tissue culture supernatants were used to infect fresh Vero cells. At 6 days postinfection (p.i.), tissue culture supernatants were collected, aliquoted, stored at −80°C, and used for viral titration using an immunofocus assay (fluorescent focus-forming units [FFU] per milliliter). Viral titrations of r3TCRV and rTCRV/GFP were performed by counting GFP-positive cells.

RT-PCR. Total RNA from TCRV- and rTCRV-infected (MOI = 1) Vero cells (10^6 cells/well, 6-well plate format) was extracted with TRIzol reagent (Thermo Fisher) according to the manufacturer's instructions. RT-PCR amplification of the L region spanning nt 4427 to 6188, or L-IGR, was performed by using Super Script II reverse transcriptase (Thermo Fisher) and an Expand high-fidelity PCR system (Sigma-Aldrich). The amplified 1,762 L PCR products were digested with BbsI. Amplified DNA products, undigested or digested with BbsI, were subjected to 0.7% agarose gel electrophoresis and photographed using a ChemiDoc MP imaging system (Bio-Rad). Gel-purified L fragments were subjected to Sanger sequencing (ACGT).

Plaque assays and immunostaining. Confluent monolayers of Vero cells (10^6 cells/well, 6-well plate format, triplicates) were infected with 10-fold serial dilutions of TCRV/WT, rTCRV, r3TCRV, rTCRV/GFP, or rTCRV/Δ39 for 1 h at 37°C. After viral infection, cells were overlaid with 1% low-melting-point agar and incubated at 37°C. At 6 days p.i., cells were fixed overnight with 4% PFA and the overlaid agar was removed. For visualization of GFP, PBS was added, and plates were imaged with a ChemiDoc MP imaging system (Bio-Rad) and colored using Adobe Photoshop CS software. For immunostaining, cells were permeabilized with 0.5% (vol/vol) Triton X-100 in PBS for 15 min at room temperature and immunostained as previously described (40) using the JUNV NP monoclonal antibody (1 μg/ml) and the Vectastain avidin-biotin complex kit (Vector Laboratories), following the manufacturers' instructions. After immunostaining, plates were scanned and photographed using a ChemiDoc MP imaging system (Bio-Rad).

Virus growth kinetics. Confluent monolayers of Vero cells (10^6 cells/well, 6-well plate format, triplicates) were infected (MOI = 0.01) with TCRV/WT, rTCRV, r3TCRV, rTCRV/GFP, or rTCRV/Δ39. After 1 h of virus adsorption at 37°C, cells were washed with PBS and overlaid with DMEM containing 2% (vol/vol) FBS and incubated at 37°C. At the indicated times p.i. (24, 48, 72, 96, 120, and 144 h), viral titers in tissue culture supernatants were determined by immunofocus assay using the JUNV NP monoclonal antibody (1 μg/ml), as previously described (63). In the case of r3TCRV, Gluc in the tissue culture supernatants from infected cells was quantified using the BioLux *Gaussia* luciferase assay kit (NEB), following the manufacturers' specifications.

Prediction of TCRV L-IGR RNA secondary structure. The secondary structure of TCRV L-IGR was predicted using the RNAstructure web server (https://rna.urmc.rochester.edu/RNAstructureWeb/). Images of the RNA secondary structure were drawn using the DNAMAN program (Lynnon Biosoft).

Statistical analysis. Data representative of three independent experiments in triplicate are presented. All data are means and standard deviations (SD) for each group, analyzed by SPSS13.0 (IBM). A

two-tailed Student's *t* test was used to compare the means between two groups. *P* values less than 0.05 were considered statistically significant.

Data availability. TCRV S and L viral segment sequences have been deposited in GenBank under accession numbers MT478051 and MT478050, respectively. All primer sequences, including those used for RT-PCR, are available on request.

ACKNOWLEDGMENTS

We thank BEI Resources for providing TCRV TRVL-11573 (NR-10175) and the JUNV NP monoclonal antibody PC01-AD12 (NR-2583).

This research was supported by NIAID R21 grants A1135284 (L.M.-S.) and AI121840 (J.C.T.), NIAID RO1 grant AI132443 (J.C.T. and L.M.-S.), and Department of Defense (DoD) Peer Reviewed Medical Research Program (PRMRP) grants W81XWH-18-1-0071 (L.M.-S.) and W81XWH-19-1-0496 (L.M.-S.).

REFERENCES

1. Gonzalez J-P, Emonet S, De Lamballerie X, Charrel R. 2007. Arenaviruses. Curr Top Microbiol Immunol 315:253–288. https://doi.org/10.1007/978-3-540-70962-6_11.
2. Wilson SM, Clegg J. 1991. Sequence analysis of the S RNA of the African Arenavirus Mopeia—an unusual secondary structure feature in the intergenic region. Virology 180:543–552. https://doi.org/10.1016/0042-6822(91)90068-M.
3. López N, Franze-Fernández MT. 2007. A single stem-loop structure in Tacaribe arenavirus intergenic region is essential for transcription termination but is not required for a correct initiation of transcription and replication. Virus Res 124:237–244. https://doi.org/10.1016/j.virusres.2006.10.007.
4. Pinschewer DD, Perez M, de la Torre JC. 2005. Dual role of the lymphocytic choriomeningitis virus intergenic region in transcription termination and virus propagation. J Virol 79:4519–4526. https://doi.org/10.1128/JVI.79.7.4519-4526.2005.
5. Radoshitzky SR, Bao Y, Buchmeier MJ, Charrel RN, Clawson AN, Clegg CS, DeRisi JL, Emonet S, Gonzalez JP, Kuhn JH, Lukashevich IS, Peters CJ, Romanowski V, Salvato MS, Stenglein MD, de la Torre JC. 2015. Past, present, and future of arenavirus taxonomy. Arch Virol 160:1851–1874. https://doi.org/10.1007/s00705-015-2418-y.
6. Beyer WR, Pöpplau D, Garten W, von Laer D, Lenz O. 2003. Endoproteolytic processing of the lymphocytic choriomeningitis virus glycoprotein by the subtilase SKI-1/S1P. J Virol 77:2866–2872. https://doi.org/10.1128/jvi.77.5.2866-2872.2003.
7. Burri DJ, da Palma JR, Seidah NG, Zanotti G, Cendron L, Pasquato A, Kunz S. 2013. Differential recognition of Old World and New World arenavirus envelope glycoproteins by subtilisin kexin isozyme 1 (SKI-1)/site 1 protease (S1P). J Virol 87:6406–6414. https://doi.org/10.1128/JVI.00072-13.
8. Hallam SJ, Koma T, Maruyama J, Paessler S. 2018. Review of mammarenavirus biology and replication. Front Microbiol 9:1751. https://doi.org/10.3389/fmicb.2018.01751.
9. Lee KJ, Novella IS, Teng MN, Oldstone MB, de la Torre JC. 2000. NP and L proteins of lymphocytic choriomeningitis virus (LCMV) are sufficient for efficient transcription and replication of LCMV genomic RNA analogs. J Virol 74:3470–3477. https://doi.org/10.1128/jvi.74.8.3470-3477.2000.
10. Flatz L, Bergthaler A, de la Torre JC, Pinschewer DD. 2006. Recovery of an arenavirus entirely from RNA polymerase I/II-driven cDNA. Proc Natl Acad Sci U S A 103:4663–4668. https://doi.org/10.1073/pnas.0600652103.
11. Martínez-Sobrido L, Giannakas P, Cubitt B, García-Sastre A, de La Torre JC. 2007. Differential inhibition of type I interferon induction by arenavirus nucleoproteins. J Virol 81:12696–12703. https://doi.org/10.1128/JVI.00882-07.
12. Martínez-Sobrido L, Emonet S, Giannakas P, Cubitt B, García-Sastre A, Juan C. 2009. Identification of amino acid residues critical for the anti-interferon activity of the nucleoprotein of the prototypic arenavirus lymphocytic choriomeningitis virus. J Virol 83:11330–11340. https://doi.org/10.1128/JVI.00763-09.
13. Perez M, Craven RC, Juan C. 2003. The small RING finger protein Z drives arenavirus budding: implications for antiviral strategies. Proc Natl Acad Sci U S A 100:12978–12983. https://doi.org/10.1073/pnas.2133782100.
14. Cornu TI, de la Torre JC. 2001. RING finger Z protein of lymphocytic choriomeningitis virus (LCMV) inhibits transcription and RNA replication of an LCMV S-segment minigenome. J Virol 75:9415–9426. https://doi.org/10.1128/JVI.75.19.9415-9426.2001.
15. Perez M, Greenwald DL, de La Torre JC. 2004. Myristoylation of the RING finger Z protein is essential for arenavirus budding. J Virol 78:11443–11448. https://doi.org/10.1128/JVI.78.20.11443-11448.2004.
16. Fan L, Briese T, Lipkin WI. 2010. Z proteins of New World arenaviruses bind RIG-I and interfere with type I interferon induction. J Virol 84:1785–1791. https://doi.org/10.1128/JVI.01362-09.
17. Perez M, de la Torre JC. 2003. Characterization of the genomic promoter of the prototypic arenavirus lymphocytic choriomeningitis virus. J Virol 77:1184–1194. https://doi.org/10.1128/jvi.77.2.1184-1194.2003.
18. Zapata J, Salvato M. 2013. Arenavirus variations due to host-specific adaptation. Viruses 5:241–278. https://doi.org/10.3390/v5010241.
19. Charrel RN, de Lamballerie X. 2003. Arenaviruses other than Lassa virus. Antiviral Res 57:89–100. https://doi.org/10.1016/s0166-3542(02)00202-4.
20. Downs WG, Anderson CR, Spence L, Aitken THG, Greenhall AH. 1963. Tacaribe virus, a new agent isolated from Artibeus bats and mosquitoes in Trinidad, West Indies. Am J Trop Med Hyg 12:640–646. https://doi.org/10.4269/ajtmh.1963.12.640.
21. Sayler KA, Barbet AF, Chamberlain C, Clapp WL, Alleman R, Loeb JC, Lednicky JA. 2014. Isolation of Tacaribe virus, a Caribbean arenavirus, from host-seeking Amblyomma americanum ticks in Florida. PLoS One 9:e115769. https://doi.org/10.1371/journal.pone.0115769.
22. Huang C, Kolokoltsova OA, Yun NE, Seregin AV, Ronca S, Koma T, Paessler S. 2015. Highly pathogenic New World and Old World human arenaviruses induce distinct interferon responses in human cells. J Virol 89:7079–7088. https://doi.org/10.1128/JVI.00526-15.
23. Maiztegui JI, McKee KT, Barrera Oro JG, Harrison LH, Gibbs PH, Feuillade MR, Enria DA, Briggiler AM, Levis SC, Ambrosio AM, Halsey NA, Peters CJ. 1998. Protective efficacy of a live attenuated vaccine against Argentine hemorrhagic fever. J Infect Dis 177:277–283. https://doi.org/10.1086/514211.
24. McKee KT, Jr, Oro JGB, Kuehne AI, Spisso JA, Mahlandt B. 1992. Candid no. 1 Argentine hemorrhagic fever vaccine protects against lethal Junin virus challenge in rhesus macaques. Intervirology 34:154–163. https://doi.org/10.1159/000150276.
25. Dusheiko G, Nelson D, Reddy KR. 2008. Ribavirin considerations in treatment optimization. Antivir Ther 13:23–30.
26. Moreno H, Gallego I, Sevilla N, de la Torre JC, Domingo E, Martín V. 2011. Ribavirin can be mutagenic for arenaviruses. J Virol 85:7246–7255. https://doi.org/10.1128/JVI.00614-11.
27. Carballal G, Calello MA, Laguens RP, Weissenbacher MC. 1987. Tacaribe virus: a new alternative for Argentine hemorrhagic fever vaccine. J Med Virol 23:257–263. https://doi.org/10.1002/jmv.1890230308.
28. Abraham J, Kwong JA, Albarino CG, Lu JG, Radoshitzky SR, Salazar-Bravo J, Farzan M, Spiropoulou CF, Choe H. 2009. Host-species transferrin receptor 1 orthologs are cellular receptors for nonpathogenic new world clade B arenaviruses. PLoS Pathog 5:e1000358. https://doi.org/10.1371/journal.ppat.1000358.
29. Stobart CC, Moore ML. 2014. RNA virus reverse genetics and vaccine design. Viruses 6:2531–2550. https://doi.org/10.3390/v6072531.
30. Sánchez AB, Juan C. 2006. Rescue of the prototypic Arenavirus LCMV entirely from plasmid. Virology 350:370–380. https://doi.org/10.1016/j.virol.2006.01.012.
31. Albariño CG, Bird BH, Chakrabarti AK, Dodd KA, Erickson BR, Nichol ST. 2011. Efficient rescue of recombinant Lassa virus reveals the influence of

S segment noncoding regions on virus replication and virulence. J Virol 85:4020–4024. https://doi.org/10.1128/JVI.02556-10.
32. Martínez-Sobrido L, Paessler S, de la Torre JC. 2017. Lassa virus reverse genetics. Methods Mol Biol 1602:185–204. https://doi.org/10.1007/978-1-4939-6964-7_13.
33. Bergeron É, Chakrabarti AK, Bird BH, Dodd KA, McMullan LK, Spiropoulou CF, Nichol ST, Albariño CG. 2012. Reverse genetics recovery of Lujo virus and role of virus RNA secondary structures in efficient virus growth. J Virol 86:10759–10765. https://doi.org/10.1128/JVI.01144-12.
34. Emonet SF, Seregin AV, Yun NE, Poussard AL, Walker AG, Juan C, Paessler S. 2011. Rescue from cloned cDNAs and in vivo characterization of recombinant pathogenic Romero and live-attenuated Candid# 1 strains of Junin virus, the causative agent of Argentine hemorrhagic fever disease. J Virol 85:1473–1483. https://doi.org/10.1128/JVI.02102-10.
35. Lan S, McLay Schelde L, Wang J, Kumar N, Ly H, Liang Y. 2009. Development of infectious clones for virulent and avirulent pichinde viruses: a model virus to study arenavirus-induced hemorrhagic fevers. J Virol 83:6357–6362. https://doi.org/10.1128/JVI.00019-09.
36. Patterson M, Seregin A, Huang C, Kolokoltsova O, Smith J, Miller M, Smith J, Yun N, Poussard A, Grant A, Tigabu B, Walker A, Paessler S. 2014. Rescue of a recombinant Machupo virus from cloned cDNAs and in vivo characterization in interferon ($\alpha\beta/\gamma$) receptor double knockout mice. J Virol 88:1914–1923. https://doi.org/10.1128/JVI.02925-13.
37. Ortiz-Riano E, Cheng BYH, de la Torre JC, Martínez-Sobrido L. 2013. Arenavirus reverse genetics for vaccine development. J Gen Virol 94:1175–1188. https://doi.org/10.1099/vir.0.051102-0.
38. Martinez-Sobrido L, de la Torre JC. 2016. Reporter-expressing, replicating-competent recombinant Arenaviruses. Viruses 8:197. https://doi.org/10.3390/v8070197.
39. Emonet SF, Garidou L, McGavern DB, Juan C. 2009. Generation of recombinant lymphocytic choriomeningitis viruses with trisegmented genomes stably expressing two additional genes of interest. Proc Natl Acad Sci U S A 106:3473–3478. https://doi.org/10.1073/pnas.0900088106.
40. Nogales A, Baker SF, Martínez-Sobrido L. 2015. Replication-competent influenza A viruses expressing a red fluorescent protein. Virology 476:206–216. https://doi.org/10.1016/j.virol.2014.12.006.
41. Nogales A, Rodríguez-Sánchez I, Monte K, Lenschow DJ, Perez DR, Martínez-Sobrido L. 2016. Replication-competent fluorescent-expressing influenza B virus. Virus Res 213:69–81. https://doi.org/10.1016/j.virusres.2015.11.014.
42. Ngo N, Henthorn KS, Cisneros MI, Cubitt B, Iwasaki M, de la Torre JC, Lama J. 2015. Identification and mechanism of action of a novel small-molecule inhibitor of arenavirus multiplication. J Virol 89:10924–10933. https://doi.org/10.1128/JVI.01587-15.
43. Caì Y, Iwasaki M, Beitzel B, Yú S, Postnikova E, Cubitt B, DeWald L, Radoshitzky S, Bollinger L, Jahrling P, Palacios G, de la Torre J, Kuhn J. 2018. Recombinant Lassa virus expressing green fluorescent protein as a tool for high-throughput drug screens and neutralizing antibody assays. Viruses 10:655. https://doi.org/10.3390/v10110655.
44. Iwasaki M, Cubitt B, Sullivan BM, Juan C. 2016. The high degree of sequence plasticity of the arenavirus noncoding intergenic region (IGR) enables the use of a nonviral universal synthetic IGR to attenuate arenaviruses. J Virol 90:3187–3197. https://doi.org/10.1128/JVI.03145-15.
45. Iwasaki M, Ngo N, Cubitt B, Teijaro JR, Juan C. 2015. General molecular strategy for development of arenavirus live-attenuated vaccines. J Virol 89:12166–12177. https://doi.org/10.1128/JVI.02075-15.
46. Garcia JB, Morzunov SP, Levis S, Rowe J, Calderon G, Enria D, Sabattini M, Buchmeier MJ, Bowen MD, St Jeor SC. 2000. Genetic diversity of the Junin virus in Argentina: geographic and temporal patterns. Virology 272:127–136. https://doi.org/10.1006/viro.2000.0345.
47. Johnson KM, Kuns M, Mackenzie R, Webb P, Yunker C. 1966. Isolation of Machupo virus from wild rodent Calomys callosus. Am J Trop Med Hyg 15:103–106. https://doi.org/10.4269/ajtmh.1966.15.103.
48. Salas R, de Manzione N, Tesh RB, Rico-Hesse R, Shope RE, Betancourt A, Godoy O, Bruzual R, Pacheco ME, Ramos B. 1991. Venezuelan haemorrhagic fever. Lancet 338:1033–1036. https://doi.org/10.1016/0140-6736(91)91899-6.
49. Lisieux T, Coimbra M, Nassar ES, Burattini MN, de Souza LT, Ferreira I, Rocco IM, da Rosa AP, Vasconcelos PF, Pinheiro FP. 1994. New arenavirus isolated in Brazil. Lancet 343:391–392. https://doi.org/10.1016/S0140-6736(94)91226-2.
50. Delgado S, Erickson BR, Agudo R, Blair PJ, Vallejo E, Albariño CG, Vargas J, Comer JA, Rollin PE, Ksiazek TG, Olson JG, Nichol ST. 2008. Chapare virus, a newly discovered arenavirus isolated from a fatal hemorrhagic fever case in Bolivia. PLoS Pathog 4:e1000047. https://doi.org/10.1371/journal.ppat.1000047.
51. Cajimat MN, Milazzo ML, Bradley RD, Fulhorst CF. 2012. Ocozocoautla de espinosa virus and hemorrhagic fever, Mexico. Emerg Infect Dis 18:401–405. https://doi.org/10.3201/eid1803.111602.
52. Mills JN, Ellis BA, Childs JE, McKee KT, Jr, Maiztegui JI, Peters CJ, Ksiazek TG, Jahrling PB. 1994. Prevalence of infection with Junin virus in rodent populations in the epidemic area of Argentine hemorrhagic fever. Am J Trop Med Hyg 51:554–562. https://doi.org/10.4269/ajtmh.1994.51.554.
53. Contigiani M, Medeot S, Diaz G. 1993. Heterogeneity and stability characteristics of Candid 1 attenuated strain of Junin virus. Acta Virol 37:41–46.
54. Cheng BYH, Ortiz-Riaño E, Nogales A, de la Torre JC, Martínez-Sobrido L. 2015. Development of live-attenuated arenavirus vaccines based on codon deoptimization. J Virol 89:3523–3533. https://doi.org/10.1128/JVI.03401-14.
55. Cheng BY, Nogales A, de la Torre JC, Martínez-Sobrido L. 2017. Development of live-attenuated arenavirus vaccines based on codon deoptimization of the viral glycoprotein. Virology 501:35–46. https://doi.org/10.1016/j.virol.2016.11.001.
56. Cheng BYH, Ortiz-Riaño E, de la Torre JC, Martínez-Sobrido L. 2015. Arenavirus genome rearrangement for the development of live attenuated vaccines. J Virol 89:7373–7384. https://doi.org/10.1128/JVI.00307-15.
57. Golden JW, Beitzel B, Ladner JT, Mucker EM, Kwilas SA, Palacios G, Hooper JW. 2017. An attenuated Machupo virus with a disrupted L-segment intergenic region protects guinea pigs against lethal Guanarito virus infection. Sci Rep 7:4679. https://doi.org/10.1038/s41598-017-04889-x.
58. Robinson JT, Thorvaldsdóttir H, Winckler W, Guttman M, Lander ES, Getz G, Mesirov JP. 2011. Integrative genomics viewer. Nat Biotechnol 29:24–26. https://doi.org/10.1038/nbt.1754.
59. Kochs G, García-Sastre A, Martínez-Sobrido L. 2007. Multiple anti-interferon actions of the influenza A virus NS1 protein. J Virol 81:7011–7021. https://doi.org/10.1128/JVI.02581-06.
60. Hemsley A, Arnheim N, Toney MD, Cortopassi G, Galas DJ. 1989. A simple method for site-directed mutagenesis using the polymerase chain reaction. Nucleic Acids Res 17:6545–6551. https://doi.org/10.1093/nar/17.16.6545.
61. Ortiz-Riaño E, Ngo N, Devito S, Eggink D, Munger J, Shaw ML, de la Torre JC, Martínez-Sobrido L. 2014. Inhibition of arenavirus by A3, a pyrimidine biosynthesis inhibitor. J Virol 88:878–889. https://doi.org/10.1128/JVI.02275-13.
62. Cheng BY, Ortiz-Riaño E, de la Torre JC, Martínez-Sobrido L. 2013. Generation of recombinant arenavirus for vaccine development in FDA-approved Vero cells. JoVE https://doi.org/10.3791/50662.
63. Nogales A, Baker SF, Ortiz-Riaño E, Dewhurst S, Topham DJ, Martínez-Sobrido L. 2014. Influenza A virus attenuation by codon deoptimization of the NS gene for vaccine development. J Virol 88:10525–10540. https://doi.org/10.1128/JVI.01565-14.